

# Contents lists available at ScienceDirect

# Materialia

journal homepage: www.elsevier.com/locate/mtla



Full Length Article

# Evaluating the forces generated during carbon nanotube forest growth and self-assembly



Taher Hajilounezhad, Damola M. Ajiboye, Matthew R. Maschmann\*

Department of Mechanical & Aerospace Engineering, University of Missouri, Columbia, MO, USA

#### ARTICLE INFO

Keywords:
Carbon nanotubes
Mechanics
Mechanochemistry
Self-assembly
Finite element
Simulation

# ABSTRACT

The time-resolved reaction forces generated by actively growing and interacting carbon nanotube (CNT) forests are investigated using a mechanical finite element model. The CNT–CNT interaction forces are transmitted to the CNT catalyst particle residing at the base of each CNT, which may alter catalyst kinetics and modulate CNT growth rate. The simulation shows that CNTs growing at a rate greater than the population average transmit compressive force to the catalyst particle, while those growing at a slower rate transmitted tensile force. The magnitude of force for CNTs growing at a rate that was +/-10% of the population average was on the order of 100% of nanonewtons, corresponding to stress on the order of GPa. When using an Arrhenius-like kinetic model to modulate CNT growth rates, the growth rate of slower CNTs was enhanced by tensile forces, while the growth rate of faster growing CNTs was decreased by compressive forces. The net result of the force-modulation kinetics was a reaction force reduction of approximately an order of magnitude. Understanding how the growth parameters of an individual CNT are related to the mechanical forces it experiences during CNT forest assembly and the overall CNT morphology is expected to improve the control of CNT forest morphology and ensemble forest properties.

# 1. Introduction

The self-assembly of growing carbon nanotube (CNT) populations into vertically oriented forests is guided by CNT-CNT mechanical interactions between concurrently growing CNTs. CNT forests represent a scalable material suitable for thermal interfaces [1,2], electrical contacts and vias [3,4], and robust physical sensors [5–7]. While the mechanical, thermal, and electrical properties of CNT forests may exceed traditional engineering materials, their properties are significantly degraded based on a volumetric scaling of individual CNT properties [1,8-14]. The degradation of CNT forest properties likely originates from the wavy structural morphology of CNT forests [14-19] formed during the selfassembly process [17] by mechanisms currently not well understood. The chemical vapor deposition (CVD) synthesis of CNT forests typically proceeds from the base-growth mechanism in which catalyst nanoparticles support CNT formation while residing on a rigid substrate throughout the duration of growth. As a result, the forces generated by CNT forest self-assembly are transmitted directly to the catalyst particles. The magnitude of these forces as a function of CNT population attributes and their impact to the self-assembly process has yet to be thoroughly examined.

The parameter space for the CVD synthesis is vast, facilitating the synthesis of CNT forests with variable growth rates, areal density, diameter, and structural morphology. To date, the process–structure–

The mechanical modeling of CNT forests is challenging because of the complex structural morphology and the interconnectivity of CNTs within a forest. Previous studies investigating the mechanics of CNT forests have employed simplified forest geometries such as an isotropic continuum [22], array of interacting beam segments [15], distinct unit

E-mail address: maschmannm@missouri.edu (M.R. Maschmann).

property relationships governing CNT forests are not fully understood. Fundamental kinetics studies using small angle x-ray scattering (SAXS) have revealed that the areal density, alignment, and diameter distribution of CNT forests evolve with time and that CNT forest growth termination is often abrupt [17-20]. Recently, an external compressive force applied to the top surface of CNT forests was shown to decrease the ensemble forest growth rate, indicating that CNT growth kinetics are directly influenced by even relatively small external forces [21]. The forces generated by forest self-assembly and transmitted to CNT catalyst particles are expected to exceed those applied in the experiment while also manifesting as both tensile and compressive orientations. By extension, it may be assumed that the mechanical forces generated during self-assembly similarly modulate the growth rate of individual CNTs during their growth and may contribute to the abrupt growth termination of CNT forests [15,16,19,21]. Measuring the evolution of forces within a forest at the level of individual CNTs is currently inaccessible by experimental techniques and requires a simulation capable of modeling both the self-assembly process of interacting CNTs and the mechanical response resulting from these interactions.

<sup>\*</sup> Corresponding author.

cells of oriented beams [8,23], perfectly vertical and non-contacting beams [9,24], or energy relaxation-based methods that populate CNTs in a volume and allow them to interact freely via van der Waals forces [25]. These modeling approaches are sufficient for approximating the mechanical response of CNT forests. However, they cannot capture the complex mechanics of forest self-assembly or the resultant forces transmitted to catalyst nanoparticles.

Here a time-resolved finite element model was employed to comprehensively study the forces generated by growing and interacting CNTs during CNT forest synthesis. After validating the simulation with two-CNT mechanics, a series of CNT forest growth simulations were examined using increasingly complex kinetics and parametric assumptions, with emphasis placed on the force and stress transmitted to the base of each CNT, corresponding to the location of active catalyst nanoparticles. CNT forests with homogeneous diameters were simulated to determine the scaling relationship between transmitted forces and CNT diameter. Next, forests with heterogeneous CNT diameters were examined using diameter-independent growth rates compared to a diameter-dependent growth rate [26]. Finally, mechanical strain imparted to the CNT catalysts was allowed to alter the growth rate of CNTs using an Arrheniustype relationship in which compressive forces decrease CNT growth rate and tensile forces increase CNT growth rates. The observed scaling laws and mechanochemical coupling observations may be used to understand and control CNT morphology for improved CNT forest properties.

# 2. Experimental

The simulation considers the concurrent growth and self-assembly of CNT populations by evaluated mechanical equilibrium of finite frame elements at discrete time increments [27]. Each simulated CNT, comprised of numerous elements connected end-to-end, underwent base growth at discrete time increments. Interactions and bonding between neighboring CNTs were approximated by a linearized van der Waals potential. Each element node supported three mechanical degrees of freedom representing axial, transverse, and angular deformation. The CNT attributes of inner and outer diameter, modulus, orientation angle, and initial growth rate were assigned to each CNT stochastically at the beginning of the simulation based on user-defined distributions. The simulation does not consider structural imperfections of CNT walls or transient catalyst mass loss via Ostwald ripening or subsurface diffusion during growth [28,29].

The CNT population growth sequence began with the nucleation of CNTs on a planar substrate. The global stiffness matrix of the CNT population, relating CNT deformation to nodal forces, was determined by assembling and rotating the local stiffness matrix of each constituent element into a global coordinate system. A representative stiffness matrix of a typical plane frame element is shown in Fig. S1 of the Supplementary Material. Because each node contributed three mechanical degrees of freedom, each element represented a 6  $\times$  6 matrix within the global stiffness matrix. A schematic of a typical frame element assembly used to model CNT forest growth over different growth time steps is shown in Fig. S2 of the Supplementary Material.

Van der Waals interactions between adjacent nodes were found by evaluating the relative pair-wise distance between all nodes in the system. Nodes within a predefined gap of 50 nm or less (measured between the central axis of two CNTs), were assumed to experience a van der Waals attraction. To model van der Waals potential, a linear-elastic bar element was introduced between the nodes in contact. The van der Waals stiffness elements between contacting nodes were then added to the global stiffness matrix.

To facilitate the growth of each CNT in the population, the bottommost node of each CNT was displaced by a magnitude representing the growth rate and orientation angle of the CNT. The displacements of all other nodes in the system due to the stretching of the bottom-most elements was computed using the updated Lagrangian modeling approach whereby

$$\{R\}_t - \{F\}_{t-1} = [K]_t \{U\}_t \tag{1}$$

where  $\{F\}$  is a vector of internal forces,  $\{R\}$  is a vector of external forces, [K] is the global stiffness matrix,  $\{U\}$  is the nodal displacement matrix, and the subscript t represents the current time step. After determining nodal displacements for a given time step, the nodal positions were then updated by adding the computed displacements to the previous position of each node. A new time step began by updating the global stiffness matrix based on the updated nodal positions and CNT–CNT contacts, and the process repeated for a user-defined number of time steps.

Because contacting CNTs were growing at mismatched rates and angles, reaction forces were generated by CNTs in contact. The forces were presumed to be insufficient for CNT contacts to slide or break [10,15]. The reaction forces may be evaluated for each node in the simulated CNT forest by multiplying the local stiffness matrix and the appropriate nodal deformation, given by:

$$\{F\} = [k][r]\{U\} \tag{2}$$

where F denotes a force vector, k is the local stiffness matrix of the element, r is a rotation matrix to transform global coordinates into local coordinates, and U is the displacement vector expressed in global coordinates. If desired, the local forces may also be translated into the global coordinate system using the appropriate rotation matrix.

#### 3. Results and discussions

The time-resolved simulation enables the evaluation of a wide range of CNT attributes and their influence on the forces exerted during forest assembly. The development of the model framework has been reported elsewhere [27,30]. Prior to using the simulation to model large CNT populations, the forces generated by the finite element model were investigated using a simplified system comprised of two CNTs. Two continuously growing and interacting CNTs were next simulated to investigate the behavior and magnitude of forces transmitted to the base of the CNT, where the catalyst particle is assumed to reside.

# 3.1. Model validation for a two-CNT growth

Model validation utilized a cantilever beam subjected to prescribed loads such that all degrees of freedom were interrogated. In all cases, a 1  $\mu$ m long cylindrical beam with a Young's Modulus of 1 TPa, outer diameter of 20 nm, and inner diameter of 14 nm served as the physical CNT parameters. The simulated loads and deflections agreed with analytical results, suggesting that the foundational stiffness matrix and solver of the CNT forest simulation is valid.

The time-resolved interactions between two concurrently growing CNTs (20 nm O.D. and 14 nm I.D.) were then simulated to establish baseline reaction forces generated by isolated two-CNT interactions. A vertically oriented CNT grew at a rate of 50 nm per time step while an angled CNT originating 100 nm away from the vertical CNT grew at 60 nm per time step, resulting in a growth rate mismatch of 10 nm per time step between the pair. The angled CNT was oriented such that CNT-CNT contact occurred at a height of 1.25 µm from the growth substrate. Emphasis was placed on evaluating the axial force transmitted to the base of each CNT, as this force represented the mechanical load transmitted to catalyst particles, as examined in greater detail later. Each CNT initially grew unconstrained in a straight line at a prescribed angle and rate. Upon contact with a neighboring CNT, the CNTs were locally bonded by van der Waals interactions. The CNT pair then bent away from the faster growing CNT with increased interaction time. The axial force imparted to the base of each CNT spiked upon the establishment of the CNT-CNT contact. The time-resolved CNT morphology and axial force measured at the base of each CNT are shown in Fig. 1. This simulation setup is similar to experimental findings from recent E-TEM results [31] in which mechanically coupling between CNTs growing at

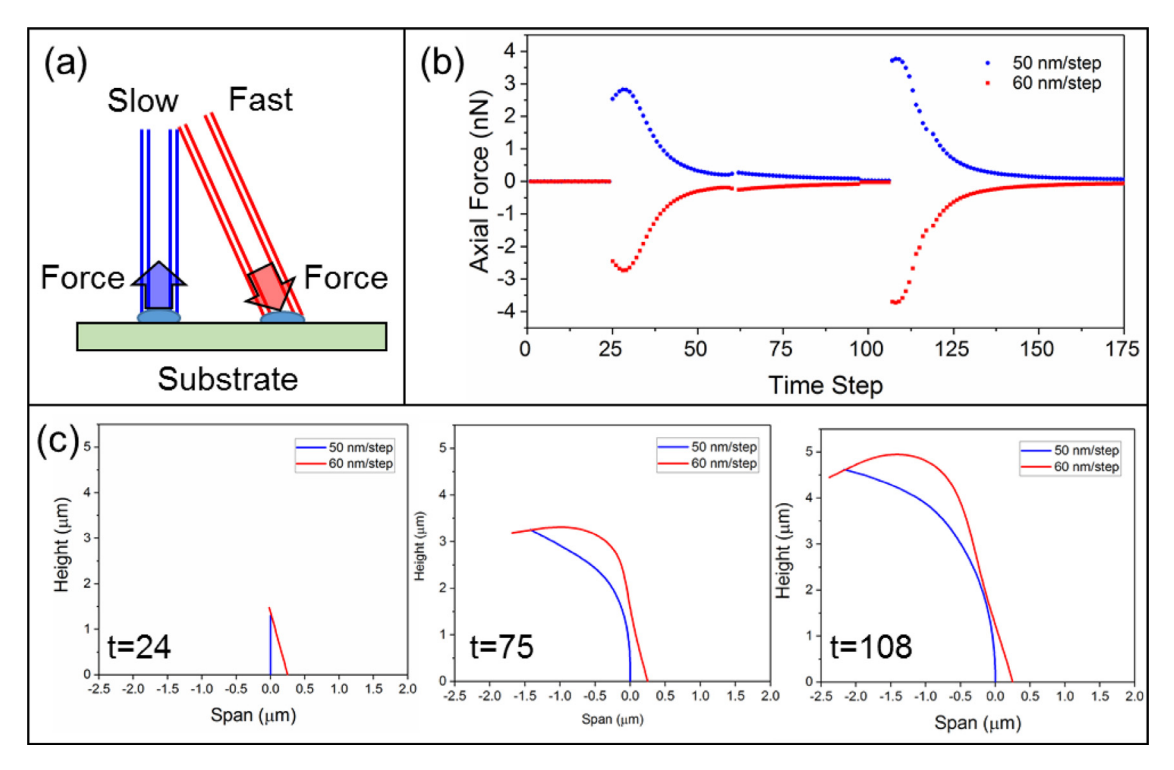


**Fig. 1.** Time-resolved axial forces transmitted to the base of CNTs. (a) A schematic depicting the direction of forces transmitted to the catalyst particle residing on a rigid substrate. (b) Time-resolved force evolution for two CNTs growing at 50 and 60 nm/step. (c)The morphology of 2 interacting CNTs shown at 24 (first contact), 75 and 108 time steps.

different rates is observed. The magnitude of the axial force generally diminished as the CNTs lengthened with time. For the simulated conditions, the maximum magnitude of force was approximately 3-4 nN, corresponding to an axial stress of 19-25 MPa. The slower-growing CNT was pulled upward by the faster growing CNT, imparting tensile loading, denoted by a positive force magnitude. Conversely, the faster growing CNT was impeded by the slower growing CNT, imparting compressive (negative magnitude) loading at its base. The magnitude of axial force reduced as the CNTs continued to lengthen. Such behavior is analogous to the force required to deflect a lengthening cantilever beam, whereby force is inversely proportional to the third power of beam length. Note that the magnitude of axial force expressed in Fig. 1 are not equal in magnitude and opposite in sign because the force vectors are aligned with the local growth axis of each individual CNT. In global coordinates, the forces are balanced at all times. Note that the forces observed between the 2-CNT interactions are validated using a static simulation with both COMSOL Multiphysics and the current CNT simulation solver, as shown in Fig. S3 and Table S1.

# 3.2. Time-resolved forces within a growing CNT forest

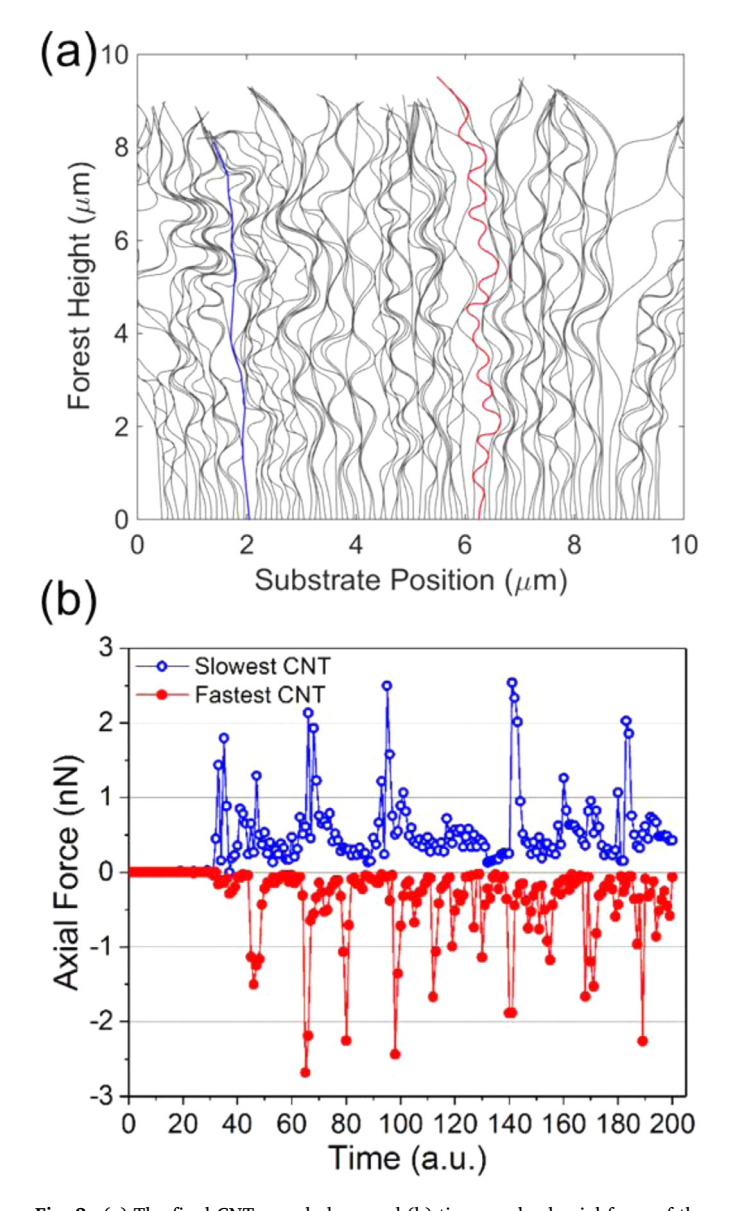
Larger CNT populations were next examined, with emphasis again placed on axial forces transmitted to the catalyst particles. Populations of 100 CNTs were grown on a 10  $\mu$ m simulation domain (10 CNT/ $\mu$ m) for a duration of 200 time steps. CNT growth rates were assigned stochastically based on a Gaussian probability density function. The average CNT growth rate was 50 nm/step with a standard deviation of 5 nm/step. For initial simulations, CNT populations were assigned a uniform outer diameter, with inner diameters equal to 70% of the outer diameters. The growth angles of the CNTs were distributed with a 5° standard deviation from the substrate normal. The mechanical force transmitted to the base of each CNT was recorded at each time step.

Fig. 2 displays the final morphology and the time-resolved axial forces transmitted to the substrate by the slowest and fastest-growing

CNT within a forest consisting of  $10\,\mathrm{nm}$  outer diameter CNTs. Note that the blue CNT in Fig. 2a represents the slowest growing CNT in the forest, while the red CNT represents the fastest growing CNT. As anticipated, the slowest-growing CNT in the forest is oriented vertically in tension, while the fastest-growing CNT demonstrates significant waviness and is bound between its two neighboring CNTs. The slowest-growing CNT does not have the back-and-forth waviness of the fastest growing CNT, but it is laterally deflected by contact with neighboring CNTs. The forces transmitted to the base of the slowest and fastest CNT within a growing population are displayed in Fig. 2b. Note that the force magnitude range experienced by the two CNTs is similar, though each have an opposite sign convention. The slowest-growing CNT is in tension at its base, while the fastest growing CNT transmits a force in compression. Each spike in force represents establishment of a new CNT-CNT connection. Note that the fastest-growing CNT experienced a greater quantity of force spikes than the slowest-growing CNT, as it more frequently contacts its neighboring CNTs. Furthermore, the slowest-growing CNT was in a constant state of non-zero tension after the initiation of contact while the fastestgrowing CNT relaxes to a nearly neutral axial force between establishment of new contacts.

# 3.3. The effect of CNT diameter

The force transmitted to the substrate was recorded for all CNTs within the population for all time steps, facilitating an evaluation of axial force as a function of each individual CNT's growth rate. A total of 10 distinct CNT forests were simulated using the same probability distribution functions for growth rate and orientation angle, and the same physical CNT parameters. CNT forests consisting of uniform CNT outer diameters of 5, 10, 20 and 40 nm were simulated for direct comparison of axial forces as a function of CNT diameter. The inner diameters were 70% of the outer diameter for all cases. Note that the 10 simulations performed for 5, 10, 20, and 40 nm diameter CNTs shared otherwise identical parameters, including growth rate and orientation assignments.



**Fig. 2.** (a) The final CNT morphology and (b) time-resolved axial force of the fastest- and slowest-growing CNTs exerted to the substrate in a 100 CNT forest. The morphology of fastest-growing (red) CNT in the forest undergoes a highly tortuous path, while the slowest-growing (blue) CNT is pulled in tension. All CNTs in the forest were assigned 10 nm outer diameter. The standard deviation of population growth rate was 5 nm per time step with a mean growth rate of 50 nm per time step.(For interpretation of the references to color in this figure legend, the reader is referred to the web version of this article.)

As observed in Fig. 2, the force transmitted to the base of each CNT varied greatly with time as the self-assembly of CNT forests proceeded and new CNT–CNT contacts were established. To examine the effect of diameter to the magnitude of forces transmitted to the catalyst particles, the time-averaged axial force for each CNT was computed after the first 50 simulation time steps. Within this sampling period, all CNTs have established contact with neighboring CNTs, ensuring that zero-force entries prior to CNT–CNT contact were not considered within the force average. The time-averaged axial force for each CNT and for all 10 simulations was plotted as a function of CNT growth rate in Fig. 3a–d. The minimum and maximum growth rate ranged from 23 to 79 nm/step. A strong negative correlation between CNT growth rate and time-averaged axial force was observed, with approximately zero average load observed at the population average growth rate of 50 nm per time step. Note that the

time-averaged forces were examined for simulation durations of up to 500 steps (see Fig. S5 of the supplementary material), with little change in the average force values; therefore, the results presented in Fig. 3 are independent of the time window over which the forces were averaged.

The magnitude of force generated within the CNT forests varied strongly with CNT diameter. The time-averaged force magnitude of data plotted in Fig. 3a–d was obtained for all forests of uniform diameter ranging from 5 to 40 nm. The resulting time-averaged force magnitude (absolute value) resulting from all simulations of like diameter is shown in Fig. 3e. CNT forests consisting of 5 nm OD CNTs produced an average force magnitude of approximately 0.25 nN, while 40 nm OD CNT forests generated average force magnitude of approximately 245 nN. The average force magnitude scales approximately as the CNT forth power of diameter, as shown by the log-plot in Fig. 3e. This scaling trend suggests that the tensile force experienced by slower-growing CNTs is generated by the bending stiffness of the faster-growing CNT population. In particular, the bending stiffness may be represented as

$$EI = \frac{\pi E}{64} \left( d_o^4 - d_i^4 \right) \tag{3}$$

where E is the Young's modulus, I is the second area moment of inertia, and  $d_o$  and  $d_i$  represent the outer and inner CNT diameter, respectively.

# 3.4. Heterogeneous CNT diameter

While CNT diameter greatly influences the magnitude of forces generated in CNT forests comprised of uniform diameter CNTs, the CNT diameters in actual CNT forests are heterogeneous rather than single-valued [16,17]. To incorporate this natural diameter variation, a Gaussian distribution of CNT outer diameters in the range of 4–16 nm [17] were introduced into simulations, with a mean value of 10 nm. The relationship between CNT diameter and CNT growth rate is uncertain for CNT forests. Puretzky et al. [26] suggested that the reaction kinetics of CNT catalyst particles is diameter dependent, whereby larger-diameter CNTs grow more quickly than smaller-diameter CNTs. This kinetic model is incorporated into the current simulations using a quadratic function, similar to recent work [15]

Growth Rate = 
$$f(0.11d^2 - 0.02d + 0.36)$$
 (4)

where d is outer diameter of each CNT and f is a scaling function. Note that the growth rate increases nonlinearly with diameter in this model. On the other hand, in-situ CNT synthesis observations of Yoshida et al. [32] indicate that growth rate is diameter-independent. Because of the uncertainty between CNT diameter and growth rate, two distinct CNT forests were simulated with exactly same inputs except for the relationship between CNT outer diameter and growth rate, i.e. diameter-dependent and diameter-independent growth rates.

Introducing heterogeneous CNT diameters into a simulation is expected to alter the magnitude and distribution of forces transmitted to the base of the CNTs. Two sets of simulations were executed using two different assumptions about how CNT growth rate was influenced by CNT diameter. Diameter-dependent growth rates were directly calculated using Eq. (4). Diameter-independent growth rates used the same set of growth rates as the diameter-dependent growth; however, the diameters and growth rates were randomly paired with no correlation. The typical growth rates for CNT outer diameters between 4 and 16 ranged from approximately 10-90 nm/step, with an average growth rate of approximately 37 nm/step. The resulting CNT morphologies were similar after 2000 growth steps, as shown in Fig. 4. Histograms of the diameter distribution and growth rate and a plot showing the growth rate as a function of CNT outer diameter may be found in Fig. S6 of the supplementary material. Similar simulations were then executed in which all parameters were identical except for the assignment of growth rate. In these diameter-independent growth rate simulations, the same growth rates used in the diameter-dependent growth rates were then randomly assigned to the CNTs in the forest, regardless of their diameter. In this way the simulations were identical in all ways except for the relationship

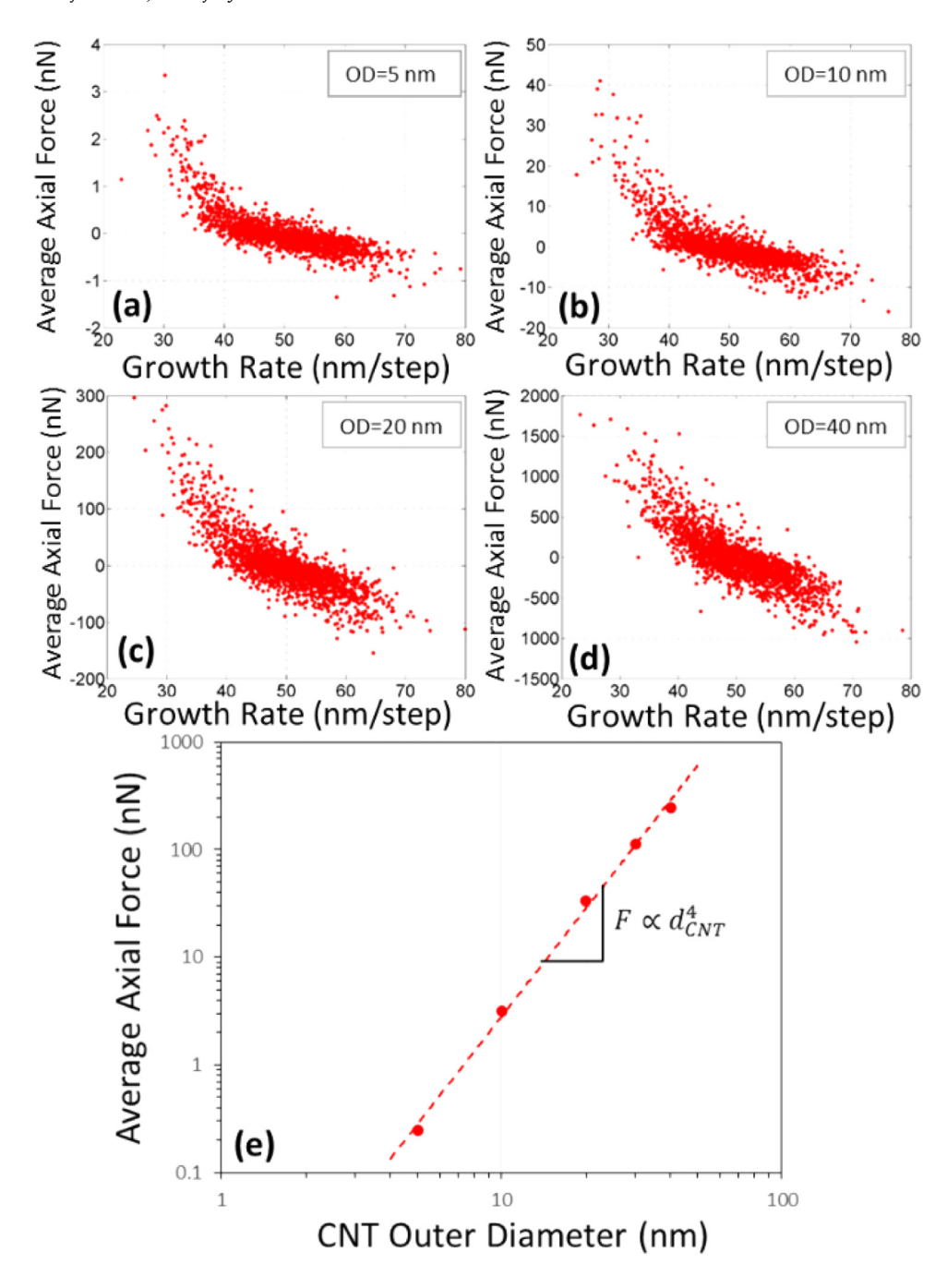


Fig. 3. The time-averaged axial force transmitted to the base of growing CNTs as a function of the CNT growth rate and diameter. The average axial force transmitted to the CNT base as a function of CNT growth rate for populations with a homogeneous outer diameter of (a) 5 nm, (b) 10 nm, (c) 20 nm, and (d) 40 nm. (e) The average axial force magnitude scales approximately as CNT outer diameter to the forth power.

in which growth rates were assigned to CNT diameters. The simulations were run for 250 time steps on a 50  $\mu m$  wide domain using 500 CNTs. 100 simulation of each type were performed, with the axial forces transmitted to the catalyst particles recorded and averages from time steps 50–250. The axial forces were also converted to stress to more readily account for the variations in diameter.

Fig. 5 displays the average axial force and axial stress as a function of both outer diameter and growth rate. Fig. 5a shows that the average forces ranged from almost 120 nN to -235 nN for the diameter-dependent growth rate and from approximately 320 nN to -160 nN for diameter-independent growth rate forest. Forces as a function of diameter followed a nonlinear trend for the diameter-dependent rates with a sign change from positive (tensile) to negative (compressive) forces near the average diameter of 10 nm. CNTs with diameters smaller than ensemble average diameter represent CNTs growing at a rate less than the average growth rate. These small-diameter CNTs experienced

tensile forces generated by interactions with faster-growing and larger-diameter CNTs. The larger-diameter (faster-growing) CNTs experienced compressive forces at their base for the same reason. Conversely, in simulations where CNT growth rate and diameter were uncoupled, seemingly no correlation between diameter and the directionality of force was exhibited. Rather, the envelope representing the time-averaged force magnitude increased, both in compression and tension, as a function of increasing diameter.

When these same average forces were examined versus CNT growth rate, as displayed in Fig. 5b, a negative correlation between force and growth rate was observed for both sets of data. Neutral loading was observed for both sets of data near the population averaged growth rate of 37 nm/step. Recall that the diameter-dependent model correlates a high growth rate with large-diameter CNTs. As a result, the fastest-growing CNTs also exhibit the greatest bending stiffness (Eq. (3)) and generate the largest (compressive) loads in the diameter-dependent

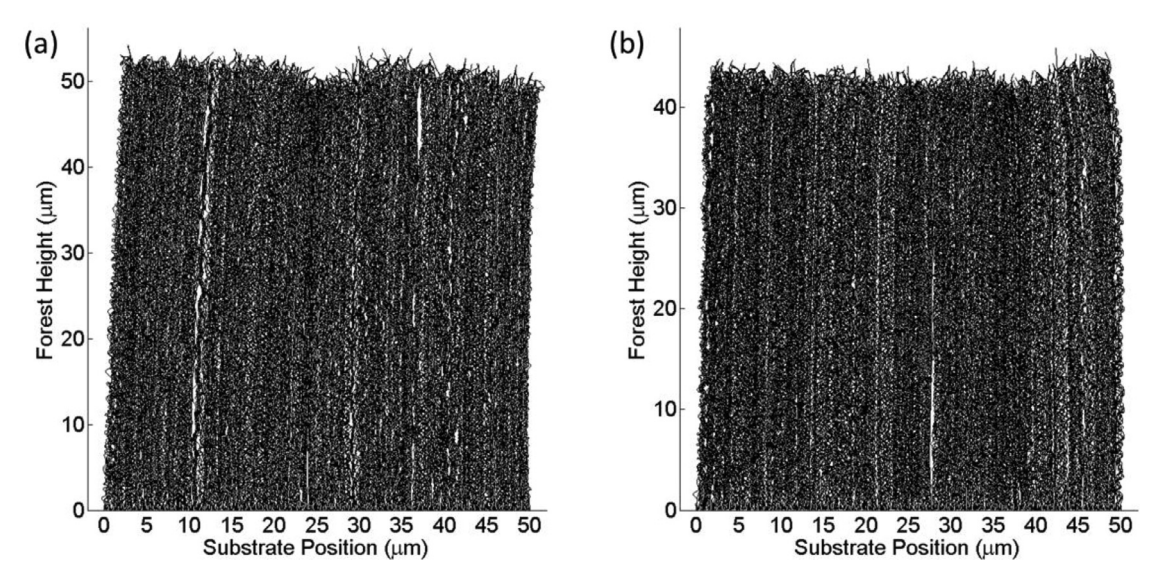


Fig. 4. Final CNT morphology of a typical 500-CNT forest featuring (a) diameter-dependent growth rates, and (b) randomly distributed, diameter-independent, growth rates after 2000 time steps.

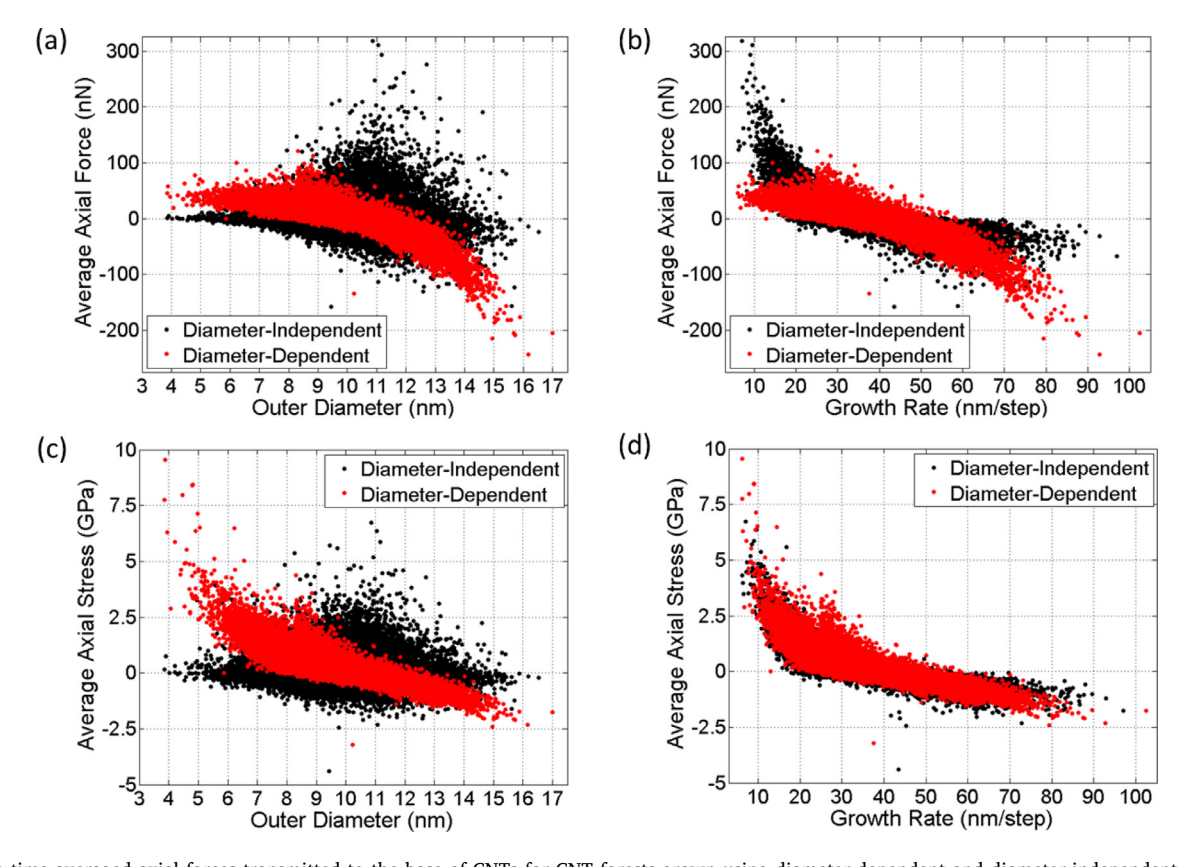


Fig. 5. The time-averaged axial forces transmitted to the base of CNTs for CNT forests grown using diameter-dependent and diameter-independent growth rates as a function of (a) CNT outer diameter (b) CNT growth rates. The time-averaged axial stress transmitted to the base of CNT forest for diameter-dependent and diameter-independent growth rates plotted as a function of (c) CNT outer diameter and (d) CNT growth rates. The data was obtained from 100 distinct simulations of each type.

growth rate model. This trend is collaborated in both Fig. 5a and b. With a diameter-independent growth rate, small-diameter CNTs may grow rapidly, generating smaller compressive loads because of a much decreased bending stiffness. In addition, the diameter-dependent growth rate model dictates that the slowest-growing CNTs in a population have the smallest diameter. The diameter-independent growth rate permits large-diameter CNTs to grow slowly. The increased tensile stiffness offered by an increased cross-sectional area decreases the tensile deformation of slow-growing CNTs while simultaneously increasing the bending

deformation of contacting CNTs. The net result of such an interaction is an increased tensile loading of slow-growing CNTs for the diameter-independent growth rate when compared to the diameter-dependent growth rate. This trend is confirmed in Fig. 5b, where the slowest-growing CNTs exhibit a load of up to 300 nN in tension.

Normalizing the axial load by the cross sectional area of the CNT converts force to axial stress, which is a more direct representation of energy density transmitted to a catalyst particle. The time-averaged axial stress for the diameter-intendent and diameter-dependent growth

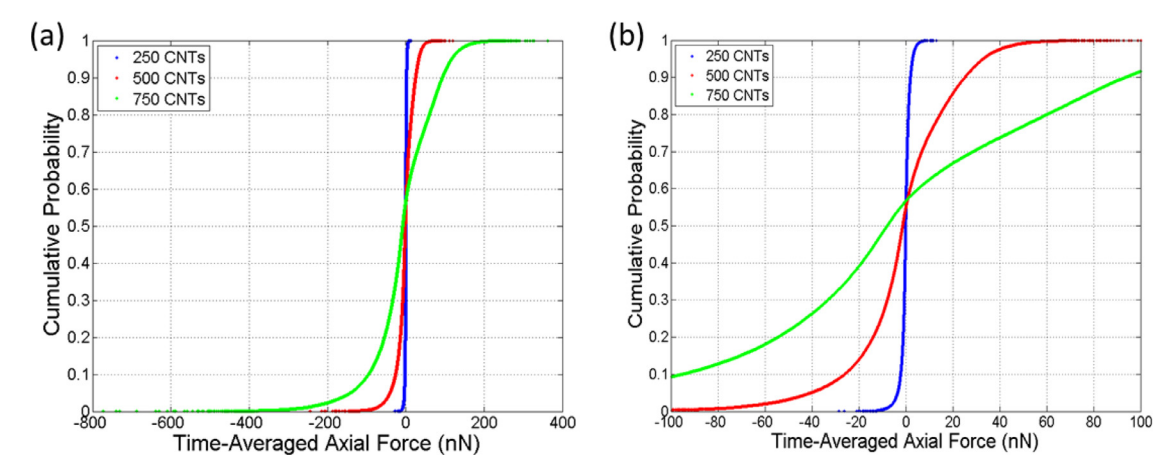


Fig. 6. The cumulative probability of axial forces generated for forests consisting of 250, 500 and 750 CNTs forests residing on a 50  $\mu$ m substrate shown for (a) the entire distribution, and (b) between -100 nN and 100 nN.

rate distributions as a function of CNT outer diameter is shown in Fig. 5c. For the parameters used in these simulations, the time-averaged stress transmitted to the catalysts ranged from -3.2 GPa to 9.5 GPa, with a majority of data residing closer to neutral stress. Interestingly, these stress values are greater than the yield strength for iron and high-strength steels, indicating that the observed stress may be sufficient to plastically deform a catalyst particle and modulate the catalytic activity. The highest tensile stress was generated in the smallest-diameter CNTs in the diameter-dependent growth rate model, as these CNTs represent the slowest-growing CNTs in the population. Interestingly, the largest magnitude of tensile and compressive stress in the diameter-independent growth rate model was near the mean diameter of 10 nm. We believe that this trend arises because of the Gaussian distribution of CNT diameters in which a large fraction of CNTs in the population resided near the average diameter. This trend was confirmed when the average stress is plotted as a function of CNT growth rate, as shown in Fig. 5d. Remarkably, the average axial stress as a function of CNT growth rate overlap for the diameter-dependent and independent growths. The overlap in results indicates that the mechanical stress transmitted from the assembling CNT forest to the catalyst particles is most strongly related to the growth rate of the individual CNT and is insensitive to the relationship between CNT diameter and growth rate. This overlap may be an artifact resulting from the quadratic nature of the diameter-dependent growth rates shown by Eq. (4). The time-averaged axial forces are divided by cross-sectional area to obtain time-averaged axial stresses. Division by the area, which also scales with the second power of diameter, may be responsible for the overlap in data. Recall that the same CNT diameters and growth rates were used for each simulation type - only the method of assigning growth rates to CNTs of different diameters differed. After many stochastic growth runs, the mechanical strain energy produced by the two growth rate models generated, on average, similar values. The results in Fig. 5d indicate that CNT growth rate is on average the dominant predictor of force transmitted to the catalyst particle, regardless of which growth rate model is used.

#### 3.5. The effect of CNT forest areal density

The areal density of CNTs is also expected to influence the magnitude of forces generated in assembling CNT forests, as the areal density will impact the frequency of CNT–CNT contacts. A set of 100 simulations each was examined in which the diameter-dependent growth rate model was implemented for cases of 250, 500 and 750 CNTs within a 50  $\mu$ m simulation domain. A similar inter-CNT spacing in a 3D CNT forest would correspond to  $2.5 \times 10^9$ ,  $10^{10}$ , and  $2.25 \times 10^{10}$  CNTs/cm², respectively. By comparison, the density of a typical CNT forest is  $10^9$ – $10^{10}$  CNTs per square centimeter [15–17]. The time-averaged forces transmitted to the catalyst particles were computed and displayed as

cumulative probability density in Fig. 6. The total simulation time was 250 time steps for each simulation, and forces were averaged between time steps 50–250.

The magnitude of force increased significantly with increased CNT density. The increase is related to an increased frequency of CNT–CNT interactions. Because the force generated by CNT–CNT interactions decays with time after the establishment of new CNT–CNT contact (see Fig. 2), an increased frequency of CNT interaction lead to increased average force. We found that the average force scaled approximately with the third power of number density. A reduced-area plot of Fig. 6a is shown in Fig. 6b. This plot demonstrates that the time averaged force axial force distribution is not symmetric, and that approximately 55–57% of CNTs are in compression, while the remainder are in tension.

### 3.6. CNT forest edge effect

Whereas CNTs in the interior of a forest incur CNT–CNT interactions from all directions, CNTs at the edges of the simulation domain may only interact with CNTs from within the interior of the forest. To investigate how this edge effect relates to the magnitude of forces transmitted to the catalyst particles, CNT densities of 250, 500, 750 CNTs over a 50  $\mu m$  substrate were simulated. Time-averaged force magnitudes were

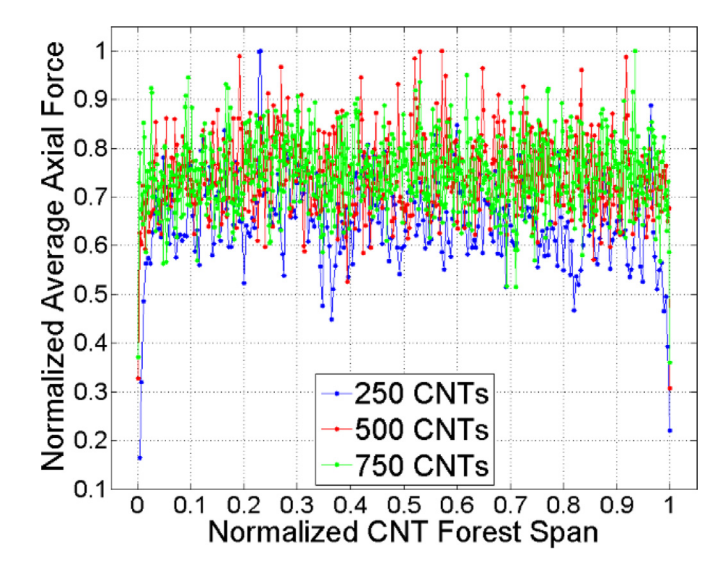


Fig. 7. Normalized magnitude of time-averaged axial force vs. normalized span for CNT forests consisting of 250, 500, and 750 CNTs within a 50  $\mu m$  simulation domain. The results are based on 100 simulations for each CNT density.

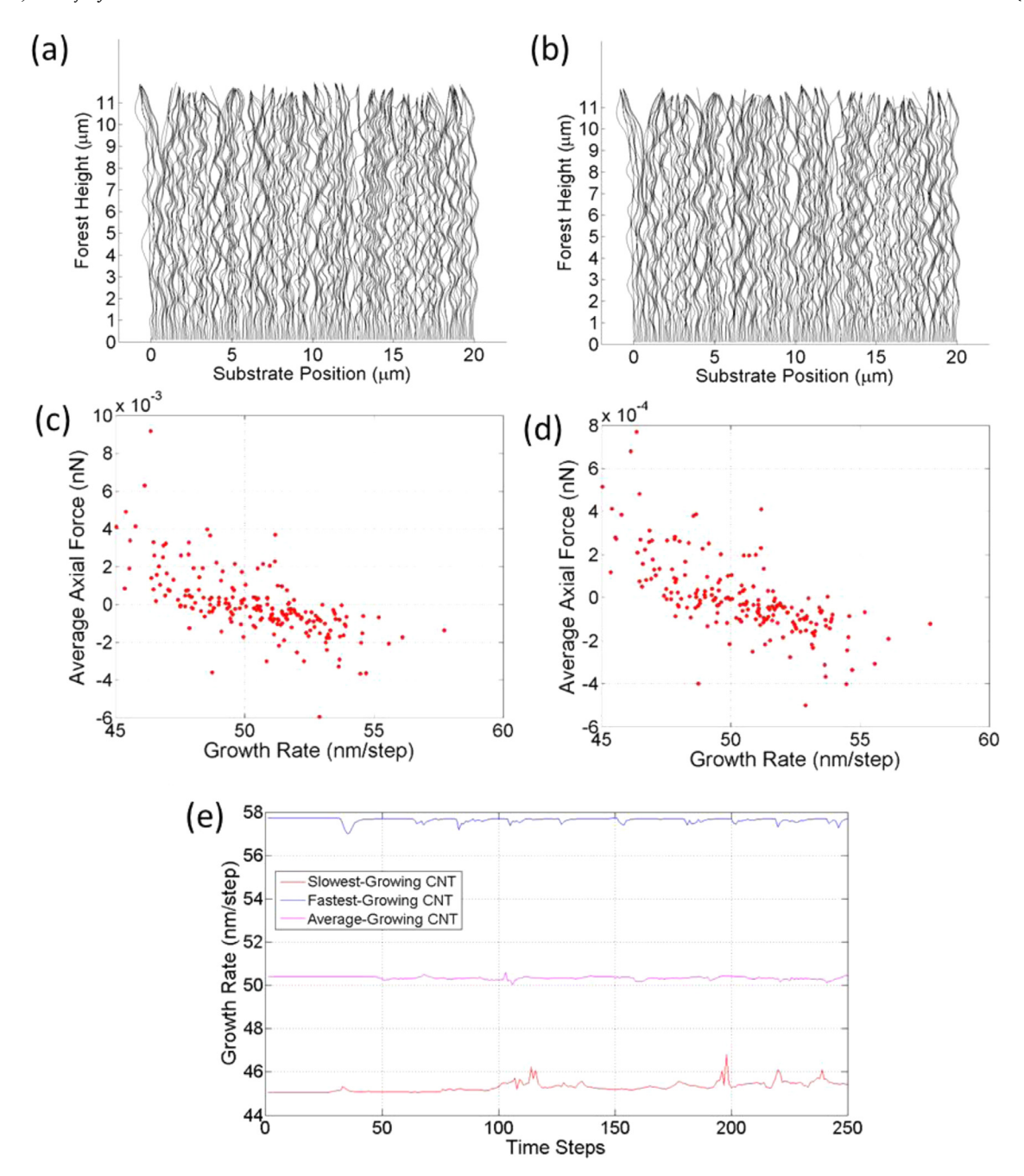


Fig. 8. A comparison of CNT forest morphology grown using (a) constant and (b) force-modulated growth rates. The time-averaged axial forces transmitted to the base of CNT forests for (c) force-independent growth rates and (d) force-modulated growth rates indicate that a force-modulated kinetic model drastically decrease the magnitude of reaction forces generated within a growing CNT forest. (e) The time-resolved CNT growth rate based on force-modulated growth rates for the slowest-growing, fastest-growing, and population average CNTs indicate that the slow-growing CNT growth rate increased with tensile forces, while fast-growing CNT growth rate decreased with compressive forces. The simulations considered a CNT forest comprised of 1 nm outer diameter CNTs simulated for 250 time steps.

recorded over 100 simulations for each configuration and were normalized based on the maximum load magnitude for each configuration. As seen in Fig. 7, the magnitude of force at the edges of the simulation are significantly less than those experienced within the interior. The transition between the edge and interior occurs over a span of 1–2  $\mu$ m, indicating that a limited "skin-effect" is present in which exterior CNTs experience reduced loading.

# 3.7. Force-modulated growth rates

The time-varying forces transmitted to CNT catalyst nanoparticles is expected to modulate the growth rate, and perhaps quality, of CNTs

within a growing forest. The role of a catalyst particle is to selectively facilitate a specific reaction pathway. Often chemical reactants are adsorbed to the surface of the catalyst particle, during which time chemical interactions between reactants and the catalyst particle act to alter the energy level of adsorbed species [33–36]. Mechanical strain modulates the interatomic displacement in a catalyst particle, thereby altering the chemical pathway of the catalytic interactions in a process known as mechanochemistry. Kinetically, mechanical strain manifests as a modification to the activation energy of a given process. Han et al. pointed out that a mechanical coupling between growing CNTs transmits forces that can create an energy barrier that ultimately exceeds energy available from chemical reaction at underlying catalyst particles [37], stunting

CNT growth. Another recent report showed that CNT forests growing under a compressive mechanical decreased the observed CNT population growth rate [21]. These studies suggest that mechanical stress acting on catalyst nanoparticles alter the activation energy of CNT growth. In these studies, the collective CNT forest grew at a decreased rate with Arrhenius-like dependence [21]:

Growth Rate = 
$$Ae^{-(E_a - \Delta E_a)/kT}$$
 (5)

where A is a constant derived when no force is applied to the substrate,  $E_a$  is the effective activation energy of CNT growth under no mechanical load which is assumed to be constant for our simulations, k is the Boltzmann constant, and T is temperature. The  $\Delta E_a$  represents a change in the activation energy resulting from mechanical energy acting on the catalyst in which tensile force is positive in sign, and compressive force is negative. The change in activation energy is linearly related to real-time applied force per CNT by a constant,  $\alpha$ .

$$\Delta E_a = \alpha F \tag{6}$$

A constant value of  $\alpha$  = 0.15 nm was found to match population-based data. Note that Eq. (6) does not account for variable CNT diameter, although the change in activation energy would likely vary as a function of strain energy, which is area-dependent. The effective activation energy for CNT growth in thermal CVD processes is in the range of 1.02–2.0 eV [17,38–40].  $\Delta Ea$  was calculated for each CNT in every time step to account for real-time forces exerted on catalyst particles. A stress-induced energy change of 0.02–0.16 eV was measured based on a compressive force application ranging from 10 pN to 1nN per CNT [21]. The study was conducted on CNT forests having diameters ranging from 6 to 10 nm and an areal density range of  $7 \times 10^8$  to  $2 \times 10^{10}$  CNTs/cm<sup>2</sup> [21]. Because the external load was applied to the entire CNT forest population, it is unclear how the loading condition of individual CNTs within the forest were affected.

This mechanochemical coupling was incorporated into the finite element model based on these experimental findings. An activation energy of 1.5 eV was selected for all simulations. If the relationship provided by Eq. (6) is to be enforced with a value of  $\alpha = 0.15$  nm, then the stability of the simulation can only be ensured by real-time CNT forces on the order of 1 nN or less. To accommodate this limited force range, CNT forests having a homogenous outer diameter of 1 nm were selected for simulation. Furthermore, Eq. (5) was strictly enforced with both compressive and tensile forces. As a result, compressive forces decreased the growth rate of CNTs, while tensile forces increased the growth rate of CNTs. Two CNT forests were simulated up to 250 time steps employing a constant outer diameter of 1 nm to explore the effect of forcemodulated growth rates during active growth. One simulation utilized force-independent CNT growth rates, while the other simulation used force-modulated growth rates based on Eq. (5-6). The simulations were otherwise identical.

Fig. 8 shows the CNT forest morphology and time-averaged axial force behavior using both force-independent and force-modulated growth rates. As displayed in Fig. 8a-b, the CNT forests grown with and without force-modulated growth rates have a similar morphology. Because the change in activation energy tends to decrease the growth rate of faster-growing CNTs (those in compression) and increase the growth rate of slower-growing CNTs (those in tension), the force modulation model tends to alter growth rates towards a population average growth rate and reduce the magnitude of forces generated within the forest. In fact, the time-averaged force transmitted to catalyst particles decreased by approximately one order of magnitude when force-modulated growth rates are considered, as shown in Fig. 8c-d. To further illustrate the modulation of CNT growth rate with time, the CNTs having the slowest and fastest initial rate as well as a CNT having a population average initial growth rate of 50 nm/step, are plotted in Fig. 8e as a function of simulation time. The forces generated by the CNT interactions are sufficient to vary the growth rate of CNTs by approximately 1 nm/step for the slowest and fastest growing CNTs. Note that the fastest-growing CNT decreases growth rate with interactions, and the slowest-growing CNT increases growth rate with interactions, as expected. By contrast, the CNT having the population-average initial growth rate experiences both increases and decreases in growth rate, as interactions are both tensile and compressive in nature. The self-modulating behavior of growth rate over time shown in Fig. 8e is in agreement with findings from [37]. We note that the force-modulated growth rate model used here, represented by Eq. (5), (6), was derived from the application of relatively small compressive force to the top surface of growing CNT forests, and further research is required to predict a more suitable mechanochemical kinetics model. Nevertheless, the force-modulation of CNT growth rate is shown to greatly impact the forces generated during the CNT forest growth assembly process and may present an opportunity for enhanced control of CNT forest properties.

#### 4. Conclusions

The time-resolved mechanical forces generated by the self-assembly of CNT forests were simulated with a finite element code, with an emphasis placed on the axial force transmitted to catalyst nanoparticles residing at the base of CNTs. We found that these axial forces were strongly correlated to CNT forest parameters including CNT diameter, areal density, and growth rate. CNTs with growth rates less than average growth rate experienced tensile loads while those with faster growth rates exerted compressive forces to catalyst particles residing on the substrate. The magnitude of forces scaled with the forth power of CNT outer diameter and the third power of areal density. Further, we found that CNTs at the physical boundary of CNT forests experience a reduction in force magnitude relative to CNTs located within the interior of a forest, as fewer CNTs are available to generate CNT-CNT reaction forces. Two distinct models were used to investigate CNT forests comprised of heterogeneous CNT diameters. One model considered a positive correlation between CNT diameter and growth rate, while the other assumed that growth rate and diameter were decoupled. Both methods produced similar CNT morphologies, and the time-averaged axial stresses between the two models followed a similar trend when plotted as a function of CNT growth rate. Finally, a mechanochemical kinetic coupling was introduced in which force transmitted to a catalyst particle altered its activation energy and subsequent CNT growth rate. The rate modulation decreased the magnitude of forces within the forest, as it decreased the growth rate of relatively fast growing CNTs and increased the growth rate of relatively slowly growing CNTs within the forest. Future studies may investigate the role of mechanochemistry in the abrupt termination of CNT forest growth. Understanding and controlling the forces generated during CNT forest self-assembly could lead to application-specific CNT forest property sets to broaden the adoption of CNT forests in engineering applications.

# **Declaration of interests**

The authors declare that they have no known competing financial interests or personal relationships that could have appeared to influence the work reported in this paper.

# Acknowledgments

The authors would like to acknowledge funding from National Science Foundation (NSF) under award CMMI 1651538.

#### Supplementary materials

Supplementary material associated with this article can be found, in the online version, at doi:10.1016/j.mtla.2019.100371.

#### References

- B.A. Cola, X. Xu, T.S. Fisher, Increased real contact in thermal interfaces: a carbon nanotube/foil material, Appl. Phys. Lett. 90 (9) (2007) 093513.
- [2] J. Xu, T.S. Fisher, Enhancement of thermal interface materials with carbon nanotube arrays, Int. J. Heat Mass Transf. 49 (9–10) (2006) 1658–1666.
- [3] N. Mizuhisa, K. Akio, K. Daiyu, H. Masahiro, S. Shintaro, A. Yuji, Electrical properties of carbon nanotube bundles for future via interconnects, Jpn. J. Appl. Phys. 44 (4R) (2005) 1626.
- [4] M. Park, B.A. Cola, T. Siegmund, J. Xu, M.R. Maschmann, T.S. Fisher, H. Kim, Effects of a carbon nanotube layer on electrical contact resistance between copper substrates, Nanotechnology 17 (9) (2006) 2294–2303.
- [5] M.R. Maschmann, B. Dickinson, G.J. Ehlert, J.W. Baur, Force sensitive carbon nanotube arrays for biologically inspired airflow sensing, J. Smart Mater. Struct. 21 (9) (2012) 094024.
- [6] M.R. Maschmann, G.J. Ehlert, B.T. Dickinson, D.M. Phillips, C.W. Ray, G.W. Reich, J.W. Baur, Bioinspired carbon nanotube fuzzy fiber hair sensor for air-flow detection, Adv. Mater. 26 (20) (2014) 3230–3234.
- [7] T. Yamada, Y. Hayamizu, Y. Yamamoto, Y. Yomogida, A. Izadi-Najafabadi, D.N. Futaba, K. Hata, A stretchable carbon nanotube strain sensor for human-motion detection. Nat. Nanotechnol. 6 (2011) 296.
- [8] Y. Gao, T. Kodama, Y. Won, S. Dogbe, L. Pan, K.E. Goodson, Impact of nanotube density and alignment on the elastic modulus near the top and base surfaces of aligned multi-walled carbon nanotube films. Carbon 50 (10) (2012) 3789–3798.
- [9] A. Cao, P.L. Dickrell, W.G. Sawyer, M.N. Ghasemi-Nejhad, P.M. Ajayan, Super-compressible foamlike carbon nanotube films, Science 310 (5752) (2005) 1307–1310.
- [10] M.R. Maschmann, G.J. Ehlert, S.J. Park, D. Mollenhauer, B. Maruyama, A.J. Hart, J.W. Baur, Visualizing strain evolution and coordinated buckling within CNT arrays by in situ digital image correlation, Adv. Funct. Mater. 22 (22) (2012) 4686–4695.
- [11] M.F. De Volder, S.H. Tawfick, R.H. Baughman, A.J. Hart, Carbon nanotubes: present and future commercial applications, Science 339 (6119) (2013) 535–539.
- [12] M.R. Maschmann, G.J. Ehlert, B.T. Dickinson, D.M. Phillips, C.W. Ray, G.W. Reich, J.W.J.A.M. Baur, Bioinspired carbon nanotube fuzzy fiber hair sensor for air-flow detection, Adv. Mater. 26 (20) (2014) 3230–3234.
- [13] M.R. Maschmann, Q. Zhang, F. Du, L. Dai, J. Baur, Length dependent foam-like mechanical response of axially indented vertically oriented carbon nanotube arrays, Carbon 49 (2) (2011) 386–397.
- [14] S.B. Hutchens, L.J. Hall, J.R. Greer, In situ mechanical testing reveals periodic buckle nucleation and propagation in carbon nanotube bundles, Adv. Funct. Mater. 20 (14) (2010) 2338–2346.
- [15] M. Bedewy, A.J. Hart, Mechanical coupling limits the density and quality of self-organized carbon nanotube growth, Nanoscale 5 (7) (2013) 2928–2937.
- [16] M. Bedewy, E.R. Meshot, M.J. Reinker, A.J. Hart, Population growth dynamics of carbon nanotubes, ACS Nano 5 (11) (2011) 8974–8989.
- [17] M. Bedewy, E. Meshot, H. Guo, E. Verploegen, W. Lu, A.J. Hart, Collective mechanism for the evolution and self-termination of vertically aligned carbon nanotube growth, J. Phys. Chem. C 113 (48) (2009) 20576–20582.
- [18] E.R. Meshot, M. Bedewy, K.M. Lyons, A.R. Woll, K.A. Juggernauth, S. Tawfick, A.J. Hart, Measuring the lengthening kinetics of aligned nanostructures by spatiotemporal correlation of height and orientation, Nanoscale 2 (6) (2010) 896–900.
- [19] E.R. Meshot, A.J. Hart, Abrupt self-termination of vertically aligned carbon nanotube growth, Appl. Phys. Lett. 92 (11) (2008) 113107.
- [20] E.R. Meshot, E. Verploegen, M. Bedewy, S. Tawfick, A.R. Woll, K.S. Green, M. Hromalik, L.J. Koerner, H.T. Philipp, M.W. Tate, High-speed in situ X-ray scattering of carbon nanotube film nucleation and self-organization, ACS Nano 6 (6) (2012) 5091–5101
- [21] N.T. Dee, M. Bedewy, A. Rao, J. Beroz, B. Lee, E.R. Meshot, C.A.C. Chazot, P.R. Kidambi, H. Zhao, T. Serbowicz, K. Teichert, P.K. Purohit, A.J. Hart, In situ mechanochemical modulation of carbon nanotube forest growth, Chem. Mater. 31 (2) (2019) 407–418.

- [22] S.B. Hutchens, A. Needleman, J.R. Greer, Analysis of uniaxial compression of vertically aligned carbon nanotubes, J. Mech. Phys. Solids 59 (10) (2011) 2227–2237.
- [23] Y. Won, Y. Gao, M.A. Panzer, R. Xiang, S. Maruyama, T.W. Kenny, W. Cai, K.E. Goodson, Zipping, entanglement, and the elastic modulus of aligned single-walled carbon nanotube films, Proc. Natl. Acad. Sci. 110 (51) (2013) 20426–20430.
- [24] M.R. Maschmann, Q. Zhang, R. Wheeler, F. Du, L. Dai, J. Baur, In situ SEM observation of column-like and foam-like CNT array nanoindentation, ACS Appl. Mater. Interfaces 3 (3) (2011) 648–653.
- [25] S. Sadasivam, S.L. Hodson, M.R. Maschmann, T.S. Fisher, Combined microstructure and heat transfer modeling of carbon nanotube thermal interface materials, J. Heat Transf. 138 (4) (2016) 042402–042402-12.
- [26] A.A. Puretzky, D.B. Geohegan, S. Jesse, I.N. Ivanov, G. Eres, In situ measurements and modeling of carbon nanotube array growth kinetics during chemical vapor deposition, Appl. Phys. A 81 (2) (2005) 223–240.
- [27] M.R. Maschmann, Integrated simulation of active carbon nanotube forest growth and mechanical compression, Carbon 86 (0) (2015) 26–37.
- [28] S. Sakurai, H. Nishino, D.N. Futaba, S. Yasuda, T. Yamada, A. Maigne, Y. Matsuo, E. Nakamura, M. Yumura, K. Hata, Role of subsurface diffusion and Ostwald ripening in catalyst formation for single-walled carbon nanotube forest growth, J. Am. Chem. Soc. 134 (4) (2012) 2148–2153.
- [29] P.B. Amama, C.L. Pint, S.M. Kim, L. McJilton, K.G. Eyink, E.A. Stach, R.H. Hauge, B. Maruyama, Influence of alumina type on the evolution and activity of aluminasupported Fe catalysts in single-walled carbon nanotube carpet growth, ACS Nano 4 (2) (2010) 895–904.
- [30] T. Hajilounezhad, M.R. Maschmann, Numerical Investigation of internal forces during carbon nanotube forest self-assembly, in: ASME 2018 International Mechanical Engineering Congress and Exposition, American Society of Mechanical Engineers, 2018 V002T02A088.
- [31] V. Balakrishnan, M. Bedewy, E.R. Meshot, S.W. Pattinson, E.S. Polsen, F. Laye, D.N. Zakharov, E.A. Stach, A.J. Hart, Real-time imaging of self-organization and mechanical competition in carbon nanotube forest growth, ACS Nano 10 (12) (2016) 11496–11504.
- [32] H. Yoshida, S. Takeda, T. Uchiyama, H. Kohno, Y. Homma, Atomic-scale in-situ observation of carbon nanotube growth from solid state iron carbide nanoparticles, Nano Lett. 8 (7) (2008) 2082–2086.
- [33] J.G. Hernandez, C. Bolm, Altering product selectivity by mechanochemistry, J. Org. Chem. 82 (8) (2017) 4007–4019.
- [34] S. Raghuraman, M.B. Elinski, J.D. Batteas, J.R. Felts, Driving surface chemistry at the nanometer scale using localized heat and stress, Nano Lett. 17 (4) (2017) 2111–2117.
- [35] B. Hammer, J.K. Nørskov, Electronic factors determining the reactivity of metal surfaces, Surf. Sci. 343 (3) (1995) 211–220.
- [36] A. Khorshidi, J. Violet, J. Hashemi, A.A. Peterson, How strain can break the scaling relations of catalysis, Nat. Catal. 1 (4) (2018) 263.
- [37] J.H. Han, R.A. Graff, B. Welch, C.P. Marsh, R. Franks, M.S. Strano, A mechanochemical model of growth termination in vertical carbon nanotube forests, ACS Nano 2 (1) (2008) 53–60.
- [38] K. Liu, K. Jiang, C. Feng, Z. Chen, S. Fan, A growth mark method for studying growth mechanism of carbon nanotube arrays, Carbon 43 (14) (2005) 2850–2856.
- [39] M.J. Bronikowski, Longer nanotubes at lower temperatures: the influence of effective activation energies on carbon nanotube growth by thermal chemical vapor deposition, J. Phys. Chem. C 111 (48) (2007) 17705–17712.
- [40] Y.T. Lee, J. Park, Y.S. Choi, H. Ryu, H.J. Lee, Temperature-dependent growth of vertically aligned carbon nanotubes in the range 800–1100°C, J. Phys. Chem. B 106 (31) (2002) 7614–7618.